Scan-Less, Kilo-Pixel, Line-Field Confocal Phase Imaging with Spectrally Encoded Dual-Comb Microscopy

Eiji Hase [ORCID], Takeo Minamikawa [ORCID], Shuji Miyamoto, Ryuji Ichikawa, Yi-Da Hsieh, Yasuhiro Mizutani, Tetsuo Iwata, Hirotsugu Yamamoto, and Takeshi Yasui [ORCID]

Abstract—Confocal laser microscopy (CLM) is a powerful tool in life science research and industrial inspection, and its image acquisition rate is boosted by scan-less imaging techniques. However, optical-intensity-based image contrast in CLM makes it difficult to visualize transparent non-fluorescent objects or reflective objects with nanometer unevenness. In this paper, we introduce an optical frequency comb (OFC) to scan-less CLM to give optical-phase-based image contrast. One-dimensional (1-D) image pixels of a sample are separately encoded onto OFC modes via 1-D spectral encoding by using OFC as an optical carrier of amplitude and phase with a vast number of discrete frequency channels. Then, line-field confocal information of amplitude and phase are decoded from mode-resolved OFC amplitude and phase spectra obtained by dual-comb spectroscopy. The proposed confocal phase imaging will further expand the applications of CLM.

Index Terms—Biomedical imaging, optical microscopy, optical interferometry.

E. Hase is with Research and Utilization Division, Japan Synchrotron Radiation Research Institute, Hyogo 679-5198, Japan, and also with JST, ERATO, MINOSHIMA Intelligent Optical Synthesizer Project, Tokushima 770-8506, Japan (e-mail: hase@spring8.or.jp).

T. Minamikawa, T. Iwata, and T. Yasui are with the Graduate School of Technology, Industrial and Social Sciences, Tokushima University, Tokushima 770-8506, Japan, and also with JST, ERATO, MINOSHIMA Intelligent Optical Synthesizer Project, Tokushima 770-8506, Japan (e-mail: minamikawa.takeo@tokushima-u.ac.jp; iwata@tokushima-u.ac.jp; yasui.takeshi@tokushima-u.ac.jp).

S. Miyamoto was with the Graduate School of Advanced Technology and Science, Tokushima University, Tokushima 770-8506, Japan, and also with JST, ERATO, MINOSHIMA Intelligent Optical Synthesizer Project, Tokushima 770-8506, Japan. He is now with SCREEN Semiconductor Solutions Company Limited, Shiga 520-2323, Japan (e-mail: shuujimiyamoto@gmail.com).

R. Ichikawa was with the Graduate School of Advanced Technology and Science, Tokushima University, Tokushima 770-8506, Japan, and also with JST, ERATO, MINOSHIMA Intelligent Optical Synthesizer Project, Tokushima 770-8506, Japan. He is now with Tsubakimoto Chain Corporation, Kyoto 610-0380, Japan (e-mail: richikawa4504@gmail.com).

Y.-D. Hsieh was with the Graduate School of Technology, Industrial and Social Sciences,Tokushima University, Tokushima 770-8506, Japan, and also with JST, ERATO, MINOSHIMA Intelligent Optical Synthesizer Project, Tokushima 770-8506, Japan. He is now with MiZ Company Limited, Kanagawa 247-0056, Japan (e-mail: heeida@gmail.com).

Y. Mizutani is with the Graduate School of Engineering, Osaka University, Osaka 565-0871, Japan, and also with JST, ERATO, MINOSHIMA Intelligent Optical Synthesizer Project, Tokushima 770-8506, Japan (e-mail: mizutani@mech.eng.osaka-u.ac.jp).

H. Yamamoto is with the Center for Optical Research and Education, Utsunomiya University, Tochigi 321-8585, Japan, and also with JST, ERATO, MINOSHIMA Intelligent Optical Synthesizer Project, Tokushima 770-8506, Japan (e-mail: hirotsugu@yamamotolab.science).

Color versions of one or more of the figures in this paper are available online at http://ieeexplore.ieee.org.

Digital Object Identifier 10.1109/JSTQE.2018.2879017

I. INTRODUCTION

OPTICAL microscopy has been widely used as a powerful tool in life science research and industrial inspection. Therefore, the development of optical microscopy has been a principal driving force in these fields. Among various types of optical microscopy, confocal laser microscopy (CLM) [1], [2] has attracted attention due to its two-dimensional (2D) or three-dimensional (3D) imaging capability with confocality, enabling a depth resolution of wavelength order and stray light elimination. Since the confocality is achieved by a conjugate relationship among a light-source pinhole, a focal point, and a detection pinhole, mechanical scanning of the focal spot is necessary to acquire the image. However, this mechanical scanning hampers the rapid image acquisition and the robustness to surrounding external disturbance, such as air turbulence or mechanical vibration.

One promising approach to achieve confocal one-dimensional (1D) imaging without the need for mechanical scanning is a spectral encoding method, namely 1D-SE-CLM [3]–[5]. In 1D-SE-CLM, 1D image of a sample is encoded onto a broad optical spectrum based on the dimensional conversion between wavelength and space while giving the confocality, and then the sample image was decoded from the image-encoded spectrum. Such 1D-SE-CLM enables the scan-less confocal 1D imaging with the rapid image acquisition rate and high robustness against external disturbances, of which the efficacy is confirmed in medical applications [6], [7] and endoscopic applications [8], [9]. In the conventional 1D-SE-CLM, the image contrast is obtained by the optical intensity, which is sensitive to absorption, scattering, or reflection of objects; however, it is difficult to give a high image contrast to transparent non-fluorescent objects or reflective objects with nanometer unevenness. If another image contrast sensitive to these objects is given in the scan-less CLM, its range of applications will be further expanded to imaging of living cells or nanometer topography of semiconductor objects.

The use of optical phase is an interesting candidate for the new image contrast in scan-less CLM because it provides in-

formation on refractive index, optical thickness, or geometrical shape and hence visualizes transparent non-fluorescent objects or reflective objects with nanometer unevenness. One possible method for the phase contrast is confocal phase-sensitive approach [10]–[12]. Since the interference occurs just only between a light that comes from the confocal volume and a parallel reference beam, each spatial mode can act as a virtual pinhole, enabling the confocal amplitude and phase imaging without the need for confocal pinholes. Its depth resolution was achieved to nanometer based on the optical phase. However, the mechanical scanning of a focal spot or a sample is still required to obtain the line image due to the point measurement. Another possible method is an interferometric confocal microscope using an array of vertical cavity surface emitting lasers (VCSELs) [13]. Although confocal phase imaging could be achieved with an integration times of 100 μs, the lateral resolution is limited by an off-axis digital holography configuration. Differential confocal microscopy is a powerful tool for nanometer axial resolution and millisecond image acquisition in the confocal imaging by converting the signal intensity variation in a linear confocal slope into the height information [14]–[16]. However, this approach also needs mechanical scanning of a focal spot or a sample for line imaging.

Comparing with those previous CLMs, 1D-SE-CLM is more promising approach for a variety of applications from the viewpoint of the non-scanning line imaging. A potential light source for the optical-phase-based contrast in 1D-SE-CLM is an optical frequency comb (OFC) [17]–[19]. OFC is composed of a vast number of discrete, regularly spaced optical frequency modes, and the optical frequency and phase of all OFC modes are secured to a frequency standard by its inherent mode-locking nature and active laser control. Furthermore, current state-of-the-art dual-comb spectroscopy, namely DCS, enables us to rapidly, precisely, and accurately acquire the mode-resolved OFC spectra of amplitude and phase without the need of any mechanical scanning [20]–[23]. Therefore, a combination of OFC with DCS gives the optical-phase-based image contrast to 1D-SE-CLM as well as the optical-intensity-based image contrast; we call it 1D spectrally encoded dual-comb microscopy or 1D-SE-DCM. In 1D-SE-DCM, after discretely encoding 1D image pixels of a sample on each OFC mode by a 1D spectral disperser, 1D confocal images of amplitude and phase are respectively decoded from mode-resolved OFC spectra of amplitude and phase based on the one-to-one correspondence between image pixels and OFC modes. Sufficient number of OFC modes enables kilo-pixel 1D imaging even with narrow spectral bandwidth. Furthermore, the optical-phase-based image contrast provides information on refractive index, optical thickness, or geometrical shape, enabling us to visualize transparent non-fluorescent objects or reflective objects with nanometer unevenness unlike the conventional intensity-based measurement. In this paper, we demonstrated a proof-of-principle experiment of scan-less, kilo-pixel, line-field confocal phase imaging by 1D-SE-DCM.

II. PRINCIPLE

Fig. 1 shows a principle of operation. After passing through a light-source pinhole, each comb mode of an input OFC is lin-
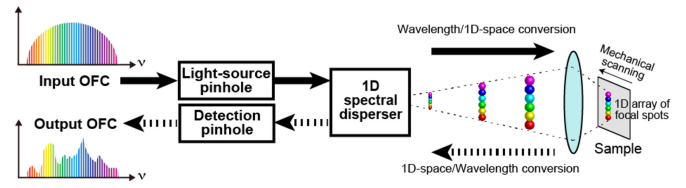

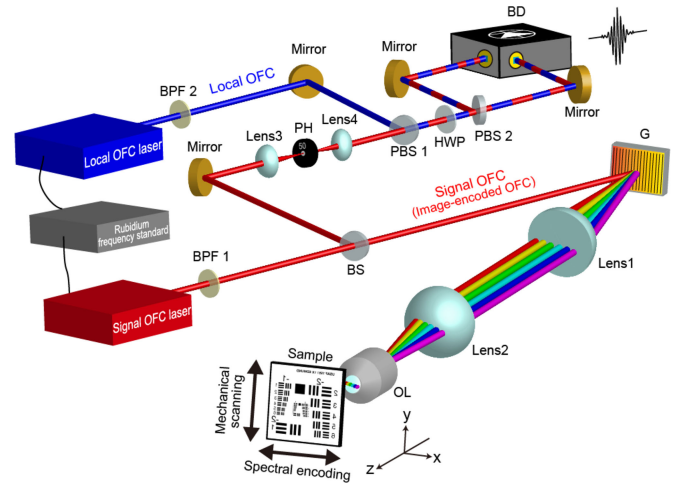Fig. 1. Principle of operation of the proposed method.

Fig. 2. Experimental setup for scan-less confocal phase imaging.

early dispersed at different angles depending on the wavelength by a 1D spectral disperser, namely wavelength/1D-space conversion. Then, spatially dispersed OFC modes are line-focused as a 1D array of focal spots onto a sample with an objective lens. Optical characteristics of a sample are encoded onto optical amplitude and phase of OFC modes when spatially dispersed OFC modes were reflected by a sample. Then, those OFC modes are spatially overlapped again by an inverse propagation of the same optics, namely 1D-space/wavelength conversion. The confocality is imposed onto the image-encoded OFC by passing through a detection pinhole. Since the mode-resolved OFC spectra of amplitude and phase reflect the 1D distribution of optical characteristics in the sample, they were acquired by DCS. Finally, 1D images of amplitude and phase are respectively reconstructed from the mode-resolved OFC spectra of amplitude and phase based on the one-to-one correspondence between image pixels and OFC modes.

III. EXPERIMENTAL SETUP

Fig. 2 shows a schematic diagram of the experimental setup. A femtosecond Er-fiber OFC laser (Menlo Systems, GmbH, Martinsried, Germany, FC1500-250, center wavelength $\lambda_c = 1550$ nm, spectral bandwidth $\Delta\lambda = 70$ nm, mean power $P = 330$ mW, repetition frequency $f_{rep1} = 250{,}001{,}484$ Hz, carrier-envelope-offset frequency $f_{ceo1} = 20{,}000{,}000$ Hz) was used as a signal OFC for 1D spectral encoding. f_{rep1} and f_{ceo1} were phase-locked to a rubidium frequency standard (Stanford Research Systems, Inc., Sunnyvale, CA, USA, FS725, accuracy = 5×10^{-11}, instability = 2×10^{-11} at 1 s) by a laser control

system. After passing through an optical bandpass filter (BPF1, passband = 1538 – 1562 nm) and a beam splitter (BS), the signal OFC light (mean power $P = 30$ mW) was diffracted by a diffraction grating (G, Spectrogon AB, Täby, Sweden, PC 1200 30 $\times$ 30 $\times$ 6, groove density: 1200 grooves/mm, efficiency: 90%). The resulting 1D spectrograph of OFC modes was relayed and then focused onto the sample along the x-direction by a pair of lenses (Lens1 and Lens2, focal length: 150 mm) and the objective lens (OL, dry, numerical aperture: 0.25, working distance: 5.5 mm, focal length: 16.6 mm). After the reflection by a sample, the signal OFC light inversely propagated the same optics for the spatial overlapping of each OFC mode, resulting in encoding of 1D image on the signal OFC spectrum. After reflecting by BS and passing through a detection pinhole (PH; diameter = 10 μm) equipped with a pair of lenses (Lens3 and Lens4; focal length = 16.6 mm), the signal OFC light was fed into the DCS system. As mentioned above, although the present method has the confocality thanks to the interference with a parallel reference beam, such "soft pinhole" has less sharp confocality than the physical pinhole or "hard pinhole". In the present experiment, we used a confocal pinhole with the interferometric configuration to benefit from both "soft" and "hard" pinholes.

We used another femtosecond Er-fiber OFC laser (Menlo Systems, GmbH, Martinsried, Germany, FC1500-250, center wavelength = 1550 nm, spectral bandwidth $\Delta\lambda = 70$ nm, mean power $P = 330$ mW, $f_{rep2} = 249,998,918$ Hz, $\Delta f_{rep} = f_{rep1} - f_{rep2} = 2,666$ Hz, $f_{ceo2} = 20,000,000$ Hz) for a local OFC. f_{rep2} and f_{ceo2} were phase-locked to the same frequency standard by another laser control system. After passing through another optical bandpass filter (BPF2, passband = 1538 – 1562 nm), the local OFC light was spatially overlapped with the signal OFC light by a polarization beam splitter (PBS1). The interferogram was detected by a combination of a half-wave plate (HWP), another polarization beam splitter (PBS2), and a balanced detector (BD, Newport Corp., Irvine, CA, USA, 1617-AC-FS, wavelength: 900-1700 nm, bandwidth: 40 kHz to 800 MHz). We acquired 10 consecutive interferograms with a time window of 40 ns at a sampling interval of 40 fs by a digitizer (Avaldata Corp., Tokyo, Japan, APX-500/ADM-214EX, sampling rate = 250,000,000 samples/s, number of sampling points = 937,735, resolution = 14 bit). The mode-resolved amplitude and phase spectra of the signal OFC were obtained by Fourier transform of the acquired interferogram, and then were used to decode the 1D amplitude and phase image of the sample. To obtain 2D image of the sample, the sample position was mechanically scanned along the y-direction perpendicular to 1D array of focal spots by a stepping-motor-driven translation stage.

We used a commercialized 1951 USAF resolution test chart with a negative pattern (Edmond Optics, Inc., Barrington, NJ, USA, #38-256) for a sample. Negative patterns were fabricated by vacuum-depositing a durable chromium coating on a float glass substrate (thickness: 1.5 mm) as a reflective film. The chromium film caused the 2D distribution of both the reflectivity and the phase change corresponding to the chart patterns.
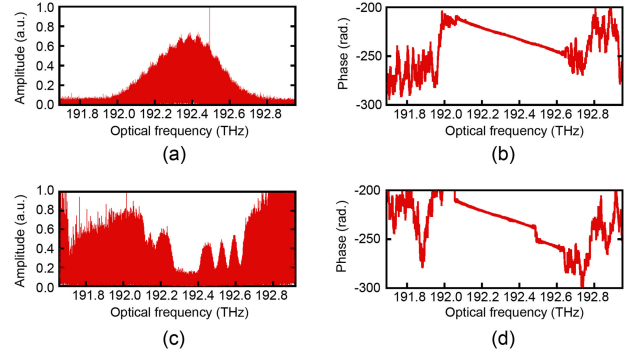

Fig. 3. Mode-resolved (a) amplitude and (b) phase spectra of the no-image-encoded OFC. Mode-resolved (c) amplitude and (d) phase spectra of the image-encoded OFC.

IV. RESULTS

A. Mode-Resolved Spectrum of Amplitude and Phase in 1D-Image-Encoded OFC

We first obtained the mode-resolved amplitude and phase spectra of the no-image-encoded OFC [Figs. 3(a) and 3(b)] and the image-encoded OFC [Figs. 3(c) and 3(d)] for the test chart. The no-image-encoded OFC and the image-encoded OFC were obtained by irradiating the signal OFC onto the no-pattern coating area and the pattern coating area of the test chart. To obtain sufficient SNR, we accumulated 5000 interferograms and then performed Fourier transform. Compared with the amplitude and phase spectra of the no-image-encoded OFC, those of the image-encoded OFC were significantly modulated. The unevenness of the spectral envelope in Figs. 3(c) and 3(d) reflects the 1D distribution of the reflectivity and phase change in the test chart, respectively. In this way, we obtained the mode-resolved spectrum of amplitude and phase in the 1D-image-encoded OFC.

B. Confocal Amplitude Imaging

To obtain 2D confocal amplitude image of the test chart, the sample position was scanned at an interval of 1 μm along the y-direction while acquiring the mode-resolved amplitude spectrum. Then, a series of the mode-resolved amplitude spectra were used for 2D confocal amplitude imaging of the test chart. Fig. 4(a) shows the confocal amplitude image of the test chart (image size = 456 μm $\times$ 150 μm, pixel size = 5000 pixels $\times$ 150 pixels), in which the horizontal dimension was decoded from the OFC spectrum of about 10 nm spectral range whereas the vertical dimension was obtained by the mechanical scanning. Several test patterns with the spatial frequency of a few tens lp/mm was clearly confirmed. The horizontal scratch patterns were mainly due to the residual timing jitter between the signal and local OFC lasers. To evaluate the spatial resolution in x-y plane or the lateral resolution δ_x, δ_y, we extracted the amplitude profile along a green line and a blue line in Fig. 4(a). Plots and lines in Figs. 4(b) and 4(c) show differential curves of amplitude profiles for these lines and the curve fitting results with a Gaussian function, respectively. When the lateral resolution is defined as a FWHM of the differential curve, δ_x and δ_y were
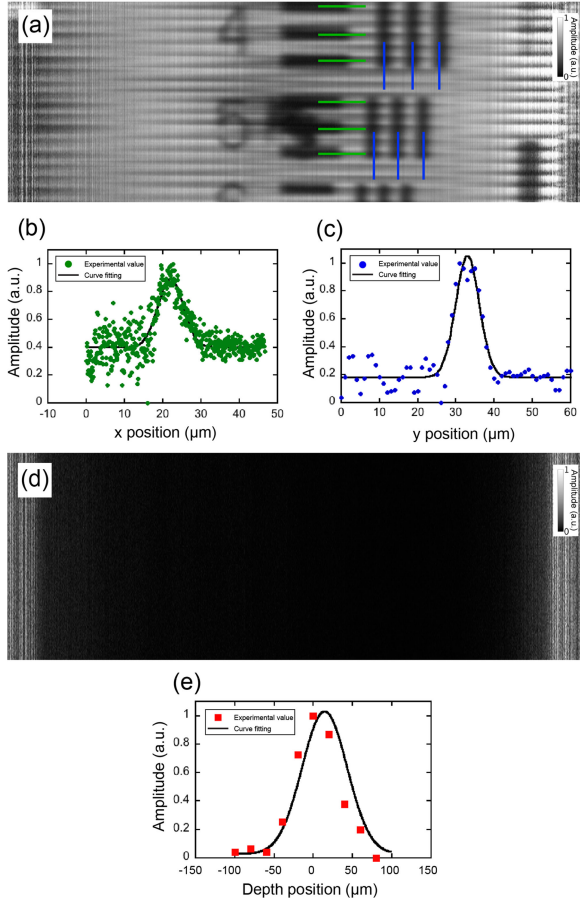
Fig. 4. (a) 2-D confocal amplitude image of a USAF resolution test chart at focus ($z = 0 \mu$m). Differential curve for lateral profiles of amplitude value along (b) x coordinate and (c) y coordinate. (d) 2-D confocal amplitude image of the test chart at out of focus ($z = +120 \mu$m). (e) Depth profiles of amplitude value with respect to the z position.

determined to be $4.9 \pm 0.2 \mu$m and $10.9 \pm 1.7 \mu$m, respectively. Since the field-of-view and the spatial resolution in x-direction were 456 μm and 4.9 μm, the effective number of resolvable points was determined to be 93 points.

To confirm the confocality in the confocal amplitude image, we set the test chart at out of focus ($z = +120 \mu$m). Fig. 4(d) shows the corresponding confocal amplitude image. The pattern of the test chart completely disappeared, implying the good confocality in the proposed 1D-SE-DCM system. For the quantitative evaluation of confocality, we measured the change of amplitude value when the sample position was incrementally moved at a step of 2 μm along z axis by a translation stage. Plots and a line in Fig. 4(e) show the depth profiles of amplitude value and the curve fitting result with a Gaussian function, respectively. From this depth profile, the depth resolution δ_z was determined to be 50.0 μm. In this way, the confocal effect was clearly confirmed in the confocal amplitude image.

C. Confocal Phase Imaging

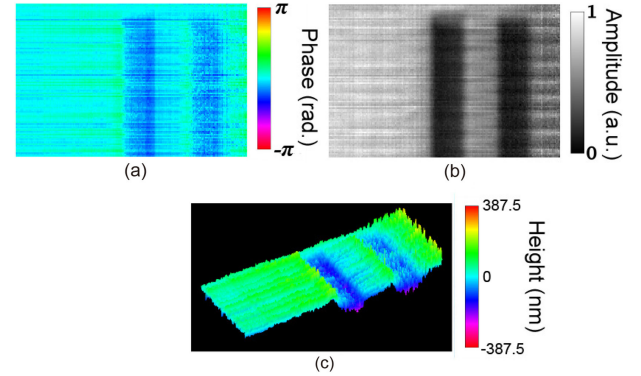Next, we decoded a confocal phase image of the test chart from the mode-resolved phase spectrum of the image-encoded

Fig. 5. (a) 2-D confocal phase image of a USAF resolution test chart at focus ($z = 0 \mu$m) and (b) the corresponding 2-D confocal amplitude image. (c) 3-D reconstructed image of the test chart calculated from the confocal phase image.

OFC. To eliminate the influence of the initial phase in the signal OFC, we subtracted the phase spectrum of the no-image-encoded OFC from that of the image-encoded OFC. Fig. 5(a) shows a confocal phase image of the test chart (image size = 190 μm $\times$ 100 μm, pixel size = 2084 pixels $\times$ 100 pixels) when we set the chart in focus ($z = 0 \mu$m), and Fig. 5(c) shows the 3D reconstructed image of Fig. 5(a). For comparison, the corresponding confocal amplitude images is shown in Fig. 5(b). Test chart pattern clearly appeared in both images. However, the image contrast mechanism is different between them: the phase difference for the confocal phase image and the reflectivity difference for the confocal amplitude image between the patterned region and the surrounding region, which are corresponding to the reflection-coated region and the uncoated region, respectively. The mean phase difference between them was determined to be 0.57 ± 0.11 rad by subtracting the mean phase value at the coated area from that at the non-coated area.

The confocal phase image in Fig. 5(a) enables us to calculate the thickness of the reflection-coating film. The relative height $H(x,y)$ is given by

$$H(x, y) = \frac{1}{2} \frac{\phi(x, y)}{2\pi} \lambda = \frac{\lambda}{4\pi} \phi(x, y) \quad (1)$$

where λ is a typical wavelength of OFC and $\Phi(x, y)$ is a confocal phase image. From the mean phase difference of 0.57 ± 0.11 rad and λ_c of 1550 nm, the mean thickness of the reflection-coating film was calculated to be 70.7 ± 13.3 nm. On the other hand, the specification value of the reflection-coating film is given to be around 100 nm. The reason for difference between the experimental value and the specification one is discussed later.

V. DISCUSSION

We first estimated the theoretical value for the lateral resolution δ_x, δ_y of the proposed 1D-SE-DCM. Theoretical δ_x and δ_y values are given by [2], [24]

$$\delta_x = \frac{f \cdot \lambda}{W} \quad (2)$$

$$\delta_y = \frac{0.61\lambda}{NA} \quad (3)$$

where f is a focal length of OL (= 16.6 mm), W is a diameter of the input beam waist (= 8 mm), and NA is a numerical aperture of OL (= 0.25). From (2) and (3), theoretical δ_x and δ_x values were estimated to be 3.2 μm and 3.8 μm, respectively. On the other hand, experimental δ_x and δ_y values were 4.9 ± 0.2 μm and 10.9 ± 1.7 μm, respectively. The beam shape was horizontally oval at the entrance pupil of the objective lens due to the reflection grating. While the x dimension of the horizontally oval shape just filled the entrance pupil of the objective lens, the y dimension of it did not fill it fully. Difference of effective NA between the x and y directions is the reason for the large difference of δ_y between the experimental and the theoretical values. The better spatial resolution will be achieved for biomedical investigation and application if a higher-NA objective lens can be used. For example, theoretical δ_x and δ_y values are estimated to be 0.64 μm and 0.74 μm by use of a water-immersion, high-NA objective lens ($NA = 1.27, f = 3.33$ mm).

We also estimated the theoretical value for the depth resolution δ_z. Theoretical δ_z value is given by [2], [24]

$$\delta_z = 0.88 \frac{\lambda}{n - \sqrt{n^2 - NA^2}} \tag{4}$$

where n is the reflective index of the medium between the objective lens and the sample (= 1). From (4), δ_z was estimated to be 43.0 μm by using NA of 0.25. This theoretical value was in good agreement with the experimental δ_z value (= 50 μm). The present experimental δ_z value is simply limited by use of low-NA objective lens. The simple way to improve the depth resolution is use of high-NA objective lens. For example, if a water-immersion, high-NA objective lens ($NA = 1.27, n = 1.33$) is used, the depth resolution of 1.46 μm can be achieved. Also, the confocal gating is another way to improve the depth resolution [10]–[13]; only the light that comes from the multiple focal points of the signal OFC is interfered with a properly collimated light of the local OFC. No use of the confocal pinhole will increase both the SNR and the depth of focus.

We next discuss the difference between the experimental value (= 70.7 ± 13.3 nm) and the specification one ($\approx$100 nm) of the reflection-coating film thickness in the test chart. When the surface unevenness is made in the same material, the phase difference is directly related to the geometrical shape. However, if the surface unevenness is made by different materials, the phase difference depends on the geometrical shape and difference of complex refractive index between different materials. Since the surface unevenness of the test chart was made by the coating film and the float glass substrate, it is corresponding the latter. When the light is normally incident on a sample, the phase shift θ of the reflected light is derived from the following equations [25], [26]

$$\hat{r} = \frac{N-1}{N+1} = \frac{n + i\kappa - 1}{n + i\kappa + 1} \equiv \sqrt{R}e^{i\theta} \tag{5}$$

$$R = \left| \frac{\sqrt{\varepsilon_r} - 1}{\sqrt{\varepsilon_r} + 1} \right|^2 = \frac{(1-n)^2 + \kappa^2}{(1+n)^2 + \kappa^2} \tag{6}$$

$$\theta = \tan^{-1} \frac{-2\kappa}{n^2 + \kappa^2 - 1} \tag{7}$$

where $\hat{r}$ is the Fresnel coefficient, N is the complex refractive index, n and κ are the real and imaginary part of the complex refractive index, R is the reflectivity, and ε_r is the dielectric constant. By substituting the complex refractive indices of the chromium ($n = 4.18$, $\kappa = 4.90$) [25] and the float glass ($n = 1.51$, $\kappa = 0$) [27] into those equations, difference of complex refractive index between the coating film and the float glass substrate results in the phase shift of -0.24 rad at the reflection. By correcting (1) with this phase shift, the final thickness of the reflection-coating film was determined to be 100.3 ± 13.3 nm, which was in good agreement with its specification value. This consistency clearly indicated a high potential of 1D-SE-DCM for nanometer surface topography.

It is important to clarify difference between the present 1D-SE-DCM and the previous 1D-SE-CLM [3], [4]. One important advantage of the present 1D-SE-DCM is the optical-phase-based image contrast although the scan-less confocal imaging can be achieved in both the 1D-SE-DCM and previous 1D-SE-CLM. Importance and usefulness of the optical-phase-based image contrast were described in the introduction and were demonstrated in the nanometer surface topography of the test chart. More interestingly, if δ_z is achieved to the phase wrapping period (λ or λ /2), the phase wrapping ambiguity, which is always an obstacle in phase imaging, can essentially be solved because the confocality suppresses the phase wrapping due to its depth selectivity. Fortunately, there is still sufficient space to decrease δ_z down to sub-micrometer by use of an oil-immersion high-NA objective lens. In this case, the combination of confocality and phase imaging, namely confocal phase imaging, will enhance the depth range from nanometer to micrometer to millimeter scale in surface topographic applications or will make it possible to visualize thick biological specimens, which introduce phase shifts of more than 2π, without the phase wrapping ambiguity.

Another advantage is a large number of pixels in the 1D image along the spectral-encoding coordinate or the x coordinate. Since the signal OFC had a spectral bandwidth $\Delta\nu$ of 1.25 THz around 192 THz, corresponding to 10.1 nm and 1550 nm in wavelength, and f_{rep} of 250 MHz, the number of pixels was achieved to 5000. On the other hand, when the similar $\Delta\nu$ was used for 1D-SE-CLM equipped with a commercialized optical spectrum analyzer (namely, OSA-based 1D-SE-CLM, spectral resolution $\approx$0.05 nm or 6.24 GHz), the number of pixels remained around 200. If a dispersive Fourier transform (parallel detection channels = 8, sampling rate of a digitizer = 50 × 10^9 sample/s) is applied for 1D-SE-CLM, namely dFT-based 1D-SE-CLM [4], [24], the number of pixels is increased up to 1600; however, it still falls short of that in 1D-SE-DCM. If 1D-SE-DCM is combined with the precise scanning of line focused beam along the y-direction, high-definition (HD) or mega-pixel 2D confocal imaging of amplitude and phase will be achieved. Also, the proposed 1D-SE-DCM has still room to increase the number of pixels up to several tens thousands by expanding $\Delta\nu$ and/or decreasing f_{rep}. Huge number of pixels enables us to expand the scan-less confocal amplitude and phase imaging to 2D imaging [28] by help of 2D spectral encoding [5], [29], [30].

One may query whether the kilo-pixel is required for 1D imaging because the present system could not optimize 5000

pixels due to its limited effective number of resolvable points (= 93). It is challenging to achieve more than 1,000 resolvable points for a commercially available microscopy objective lens. However, a combination of 8K ultra-high-definition camera with a spinning disk enables to image a 1 mm^2 field with a lateral resolution of 0.68 μm, corresponding to 1470 resolvable points [31]. Using this combination, individual activity of a single synapse was clearly visualized from the wide-field calcium imaging. Such kilo-pixel by kilo-pixel pixel wide-field imaging will be a powerful tool for biomedical imaging in the future. However, the dynamic range of signal intensity is limited to 10 bit while the wide-field imaging was performed at a frame rate of 60 fps. On the other hand, the 1D-SE-DCM has a potential to expand the dynamic range by use of a wide-dynamic-range photodetector while maintaining the similar pixels numbers.

Finally, we compare the 1D-image acquisition rate among 1D-SE-DCM, OSA-based 1D-SE-CLM, and dFT-based 1D-SE-CLM. The image acquisition rate in 1D-SE-DCM is limited by the measurement rate of DCS, which is equal to Δf_{rep} (= 2,666 Hz), and the number of signal accumulation. In the demonstration of this article, sufficient number of signal accumulation ($\approx$5000) leads to relatively slow acquisition rate (= 0.53 line/s). However, there is still space to increase the imaging speed up to Δf_{rep} without the need for the signal accumulation by using tightly-locked dual-comb sources [28]. Furthermore, the optical amplification of the image-encoded OFC by an erbium-doped fiber amplifier (EDFA) will benefit high SNR in such a single-shot measurement. The image acquisition rate in OSA-based 1D-SE-CLM is limited to around a few tens Hz due to the mechanical scanning of a diffraction grating in OSA. A combination of superluminecent diodes (SLD) with a fast spectrometer can further boost the image acquisition rate in 1D-SE-CLM up to hundreds of kHz or even over 1 MHz. However, if a sample has wavelength-dependent absorption, the broad spectrum of SLD may suffer from such absorption. Also, chromatic aberration of the objective lens is another problem. On the other hand, high spectral resolution of the 1D-SE-DCM enables the sufficient number of pixel even though a broadband light source with narrower spectral bandwidth is used. Use of such light source will reduce influence of the wavelength-dependent absorption and/or the chromatic aberration. dFT-based 1D-SE-CLM can boost the image acquisition rate up to f_{rep} (typically, a few MHz to several tens MHz) thanks to the time-stretch approach. In this way, the acquisition rate in 1D-SE-DCM is higher than that in OSA-based 1D-SE-CLM, although it could not reach that of a dFT-based 1D-SE-CLM. However, in actual fact, the maximum acquisition speed is often limited by the signal level from the sample under maximum allowable illumination power.

VI. CONCLUSIONS

We successfully introduce a new image contrast based on the optical phase to scan-less CLM by use of the 1D-image-encoding OFC with DCS. Confocal 1D images of amplitude and phase in the sample were simultaneously decoded from the mode-resolved spectra of amplitude and phase in the 1D-image-encoding OFC. Nanometer surface topography of the test chart

was demonstrated with high precision. If the image quality and image acquisition rate are further improved by reduction of the timing jitter between dual OFC lasers as well as optimization of $\Delta\nu$, f_{rep}, and Δf_{rep}, the proposed method will be a powerful tool in a variety of applications. Potential applications of the proposed method include the surface topography of semiconductor objects and non-staining 3D imaging of living cells and tissues.

REFERENCES

[1] G. J. Brakenhoff, P. Blom, and P. Barends, "Confocal scanning light microscopy with high aperture immersion lenses," *J. Microsc.*, vol. 117, no. 2, pp. 219–232, Nov. 1979.

[2] C. J. Sheppard and D. M. Shotton, "Performance of confocal microscopes," in *Confocal Laser Scanning Microscopy*, 1st ed. Oxford, U.K.: BIOS Scientific, 1997, pp. 33–44.

[3] G. J. Tearney, R. H. Webb, and B. E. Bouma, "Spectrally encoded confocal microscopy," *Opt. Lett.*, vol. 23, no. 15, pp. 1152–1154, Aug. 1998.

[4] K. K. Tsia, K. Goda, D. Capewell, and B. Jalali, "Simultaneous mechanical-scan-free confocal microscopy and laser microsurgery," *Opt. Lett.*, vol. 34, no. 14, pp. 2099–2101, Jul. 2009.

[5] K. Goda, K. K. Tsia, and B. Jalali, "Serial time-encoded amplified imaging for real-time observation of fast dynamic phenomena," *Nature*, vol. 458, pp. 1145–1150, Apr. 2009.

[6] S. C. Schlachter *et al.*, "Spectrally encoded confocal microscopy of esophageal tissues at 100 kHz line rate," *Biomed. Opt. Express*, vol. 4, no. 9, pp. 1636–1645, Aug. 2013.

[7] E. F. Brachtel *et al.*, "Spectrally encoded confocal microscopy (SECM) for diagnosing of breast cancer in excision and margin specimens," *Lab. Investigation*, vol. 96, no. 4, pp. 459–467, Apr. 2016.

[8] G. J. Tearney, M. Shishkov, and B. E. Bouma, "Spectrally encoded miniature endoscopy," *Opt. Lett.*, vol. 27, no. 6, pp. 412–414, Mar. 2002.

[9] C. Pitris, B. E. Bouma, M. Shiskov, and G. J. Tearney, "A GRISM-based probe for spectrally encoded confocal microscopy," *Opt. Express*, vol. 11, no. 6, pp. 120–124, Mar. 2003.

[10] R. L. Jungerman, P. C. D. Hobbs, and G. S. Kino, "Phase sensitive scanning optical microscope," *Appl. Phys. Lett.*, vol. 45, no. 8, pp. 846–848, Jul. 1984.

[11] T. Wilson and C. W. Shepard, *Theory and Practice of Scanning Optical Microscopy*. London, U.K.: Academic, 1984.

[12] B. T. Miles, X. Hong, and H. Gersen, "On the complex point spread function in interferometric cross-polarisation microscopy," *Opt. Express*, vol. 23, no. 2, pp. 1232–1239, Jan. 2015.

[13] B. Redding, Y. Bromberg, M. A. Choma, and H. Cao, "Full-field interferometric confocal microscopy using a VCSEL array," *Opt. Lett.*, vol. 39, no. 15, pp. 4446–4449, Aug. 2014.

[14] C. Lee and J. Wang, "Noninterferometric differential confocal microscopy with 2-nm depth resolution," *Opt. Commun.*, vol. 135, no. 4/6, pp. 233–237, Feb. 1997.

[15] C. W. Tsai, C. H. Lee, and J. Wang, "Deconvolution of local surface response from topography in nanometer profilometry with a dual-scan method," *Opt. Lett.*, vol. 27, no. 6, pp. 412–414, Mar. 2002.

[16] L. Qiu, D. Liu, W. Zhao, H. Cui, and Z. Sheng, "Real-time laser differential confocal microscopy without sample reflectivity effects," *Opt. Express*, vol. 22, no. 18, pp. 21626–21640, Sep. 2014.

[17] T. Udem, J. Reichert, R. Holzwarth, and T. W. Hänsch, "Accurate measurement of large optical frequency differences with a mode-locked laser," *Opt. Lett.*, vol. 24, no. 13, pp. 881–883, Jul. 1999.

[18] M. Niering *et al.*, "Measurement of the hydrogen 1S-2S transition frequency by phase coherent comparison with a microwave cesium fountain clock," *Phys. Rev. Lett.*, vol. 84, no. 24, pp. 5496–5499, Jun. 2000.

[19] T. Udem, R. Holzwarth, and T. W. Hänsch, "Optical frequency metrology," *Nature*, vol. 416, pp. 233–237, Mar. 2002.

[20] S. Schiller, "Spectrometry with frequency combs," *Opt. Lett.*, vol. 27, no. 9, pp. 766–768, Dec. 2002.

[21] F. Keilmann, C. Gohle, and R. Holzwarth, "Time-domain mid-infrared frequency-comb spectrometer," *Opt. Lett.*, vol. 29, no. 13, pp. 1542–1544, Jul. 2004.

[22] T. Yasui, Y. Kabetani, E. Saneyoshi, S. Yokoyama, and T. Araki, "Terahertz frequency comb by multifrequency-heterodyning photoconductive detection for high-accuracy, high-resolution terahertz spectroscopy," *Appl. Phys. Lett.*, vol. 88, no. 24, Apr. 2006, Art. no. 241104.

[23] I. Coddington, N. Newbury, and W. Swann, "Dual-comb spectroscopy," *Optica*, vol. 3, no. 4, pp. 414–426, Apr. 2016.

[24] K. K. Tsia, K. Goda, D. Capewell, and B. Jalali, "Performance of serial time-encoded amplified microscope," *Opt. Express*, vol. 18, no. 10, pp. 10016–10028, May 2010.

[25] A. D. Rakić, A. B. Djurišić, J. M. Elazar, and M. L. Majewski, "Optical properties of metallic films for vertical-cavity optoelectronic devices," *Appl. Opt.*, vol. 37, no. 22, pp. 5271–5283, Aug. 1998.

[26] L. Ward, "Theoretical background," in *The Optical Constants of Bulk Materials and Films*, 1st ed. Oxford, U.K.: Taylor & Francis, 1998, pp. 1–33.

[27] M. Rubin, "Optical properties of soda lime silica glasses," *Sol. Energy Mater.*, vol. 12, no. 4, pp. 275–288, Sep. 1985.

[28] E. Hase *et al.*, "Scan-less confocal phase imaging based on dual-comb microscopy," *Optica*, vol. 5, no. 5, pp. 634–643, May 2018.

[29] S. Xiao and A. M. Weiner, "2-D wavelength demultiplexer with potential for ≥ 1000 channels in the C-band," *Opt. Express*, vol. 12, no. 13, pp. 2895–2902, Jun. 2004.

[30] S. A. Diddams, L. Hollberg, and V. Mbele, "Molecular fingerprinting with the resolved modes of a femtosecond laser frequency comb," *Nature*, vol. 445, pp. 627–630, Feb. 2007.

[31] E. Yoshida *et al.*, "*In vivo* wide-field calcium imaging of mouse thalamocortical synapses with an 8 K ultra-high-definition camera," *Sci. Rep.*, vol. 8, May 2018, Art. no. 8324.

Eiji Hase was born in Tokushima, Japan, in 1989. He received the B.S., M.S., and Ph.D. degrees in engineering from Tokushima University, Tokushima, Japan, in 2012, 2014, and 2017, respectively.

From 2014 to 2017, he was a Research Associate with JST, ERATO, MINOSHIMA Intelligent Optical Synthesizer Project, Tokushima, Japan. Since 2017, he has been a Research Scientist with the Research and Utilization Division, Japan Synchrotron Radiation Research Institute, Hyogo, Japan, and a Visiting Associate Professor with the Graduate School of Technology, Industrial and Social Sciences, Tokushima University. His research interests include biomedical imaging and biomechanical analysis using femtosecond laser and synchrotron X-ray.

Dr. Hase was a recipient of the Optical Society of Japan Best Presentation Award 2016, Japanese Society for Medical and Biological Engineering Symposium Award 2016, and the International Society for Optical Engineering (SPIE) BiOS2016 in Photonics West 2016 Student Poster Awards in 2016. He is a Member of SPIE.

Takeo Minamikawa was born in Ibaraki, Japan, in 1983. He received the B.S., M.S., and Ph.D. degrees in engineering from Osaka University, Osaka, Japan, in 2006, 2008, and 2010, respectively.

From 2010 to 2013, he was a Research Fellow under the Research Fellowship for Young Scientists of the Japan Society for the Promotion of Science. From 2013 to 2015, he was an Assistant Professor with the Department of Pathology and Cell Regulation, Graduate School of Medical Science, Kyoto Prefectural University of Medicine, Kyoto, Japan. Since 2015, he has been an Associate Professor with the Department of Mechanical Science, Division of Science and Technology, Graduate School of Technology, Industrial and Social Sciences, Tokushima University, Tokushima, Japan. He is also with JST, ERATO, MINOSHIMA Intelligent Optical Synthesizer Project, Tokushima, Japan. He is the author of two book chapters and more than 30 articles, credited with more than 15 inventions apart from holding three patents. His research interests include Raman microspectroscopy and optical-frequency-comb.

Dr. Minamikawa is the recipient of the Japan Society for Precision Engineering Best Presentation Award 2016, Japanese Society of Pathology Poster Presentation Award 2015, and the Funai Foundation for Information Technology Research Award 2011. He is a Member of the Optical Society of America, the Japan Society of Applied Physics, the Optical Society of Japan, the Laser Society of Japan, the Japan Society of Mechanical Engineers, and the Japan Society for Precision Engineering.

Shuji Miyamoto was born in Tokushima, Japan, in 1992. He received the B.S. and M.S. degrees in mechanical engineering from Tokushima University, Tokushima, Japan, in 2015 and 2017, respectively. From 2014 to 2017, he was working on nonlinear optics under Prof. Takeshi Yasui, Tokushima University, focusing on dual-optical-comb spectroscopy and scan-less confocal microscope using broadband light source. Since 2017, he has been an Engineer with SCREEN Semiconductor Solutions Company Limited, Shiga, Japan. He is also with JST, ERATO, MINOSHIMA Intelligent Optical Synthesizer Project, Tokushima, Japan.

Mr. Miyamoto was a recipient of the Japanese Society for Medical and Biological Engineering Branch Conference Young Researcher Award in 2016.

Ryuji Ichikawa was born in Kohchi, Japan, in 1990. He received the B.S. and M.S. degrees in engineering from Tokushima University, Tokushima, Japan, in 2013 and 2015, respectively. Since 2015, he has been an Engineer with the Tsubakimoto Chain Corporation, Kyoto, Japan. He is also with JST, ERATO, MINOSHIMA Intelligent Optical Synthesizer Project, Tokushima, Japan. His research interests include THz gas spectroscopy and dual THz comb spectroscopy.

Yi-Da Hsieh was born in Kaohsiung, Taiwan, in 1984. He received the B.S. and M.S. degrees in biomedical imaging and radiological sciences from National Yang-Ming University, Taiwan, in 2006 and 2008, respectively, and the Ph.D. degree from the Graduate School of Engineering Science, Osaka University, Osaka, Japan, in 2014. From 2014 to 2016, he was a Postdoctoral Fellow with JST, ERATO, MINOSHIMA Intelligent Optical Synthesizer Project. Since 2017, he has been an Engineer with the MiZ Company Limited, Kanagawa, Japan. He is also with JST, ERATO, MINOSHIMA Intelligent Optical Synthesizer Project, Tokushima, Japan. His areas of research are THz instrumentation and optical-frequency-comb.

Yasuhiro Mizutani received the B.E. and M.E. degrees in nuclear engineering from Osaka University, Osaka, Japan, in 1997 and 1999, respectively. He obtained the Ph.D. degree in mechanical engineering from the Tokyo University of Agriculture and Technology, Tokyo, Japan, in 2008.

From 1999 to 2003, he worked as a Researcher with Panasonic Corporation. Then, from 2003 to 2009, he worked as a Research Associate with the Department of Mechanical Systems Engineering, Tokyo University of Agriculture and Technology. In 2009, he joined the University of Tokushima as an Associate Professor. Since 2015, he has been working as an Associate Professor with Osaka University. He is also with JST, ERATO, MINOSHIMA Intelligent Optical Synthesizer Project, Tokushima, Japan. He has authored or coauthored over 100 papers in refereed international journals and conferences in the areas of his research interest.

His research interests include interferometry, polarimetry, 3-D surface measurement, optical trapping, and 3-D lithography. He is a Member of the International Society for Optical Engineering and the Optical Society of America.

Tetsuo Iwata received the Ph.D. degree in engineering from Osaka University, Osaka, Japan, in 1984.

From 1984 to 1998, he worked with JASCO Corporation, Japan. He is currently a Professor with the Graduate School of Technology, Industrial and Social Sciences, Tokushima University, Tokushima, Japan. He is also with JST, ERATO, MINOSHIMA Intelligent Optical Synthesizer Project, Tokushima, Japan.

His research interests include fluorescence measurement and spectroscopy.

Hirotsugu Yamamoto received the Ph.D. degree in information science and technology from the University of Tokyo, Tokyo, Japan, in 2008.

From 1996 to 2014, he worked with Tokushima University, Tokushima, Japan. He is currently an Associate Professor in the Graduate School of Engineering, Utsunomiya University, Utsunomiya, Japan. He is also with JST, ERATO, MINOSHIMA Intelligent Optical Synthesizer Project, Tokushima, Japan.

His research interests include information photonics.

Takeshi Yasui received the first Ph.D. degree in engineering from the University of Tokushima, Tokushima, Japan, in 1997, and the second Ph.D. degree in medical science from the Nara Medical University, Yagi, Japan, in 2013.

From 1997 to 1999, he worked as a Postdoctoral Research Fellow with the National Research Laboratory of Metrology, Japan. He was with the Graduate School of Engineering Science, Osaka University from 1999 to 2010, and was briefly with the University of Bordeaux I in 2007 and 2012, and also with the University of the Littoral Opal Coast in 2010 as an Invited Professor. He is currently a Professor with the Graduate School of Technology, Industrial and Social Sciences, Tokushima University, in addition to being the Vice Director of Research Support in the same university since 2016. He is also an Invited Professor with the Graduate School of Engineering Science, Osaka University, Toyonaka, Japan. He is also with JST, ERATO, MINOSHIMA Intelligent Optical Synthesizer Project, Tokushima, Japan. His research interests include THz instrumentation and metrology, second-harmonic-generation microscopy, and optical frequency comb.

Prof. Yasui is a Member of the Optical Society of America, the International Society for Optical Engineering, the Japan Society of Applied Physics, the Optical Society of Japan, the Laser Society of Japan, the Japanese Society for Medical and Biological Engineering, and the Japan Society of Mechanical Engineers. He was a recipient of the Award for the Most Promising Young Scientist from the Optical Society of Japan in 1998, the Sakamoto Award from the Japan Society of Medical Electronics and Biological Engineering in 2006, the Optics Paper Award from the Japan Society of Applied Physics, the Funai Award from the Japan Society of Mechanical Engineers in 2009, and the Original Paper Award from the Laser Society of Japan in 2013.